Journal of
Synchrotron
Radiation

ISSN 1600-5775

Received 5 June 2014
Accepted 2 October 2014

Synchrotron radiation computed laminography using an inclined detector

Jie Zhang, Gang Li,* Qiru Yi, Yu Chen, Zhenhua Gao and Xiaoming Jiang

Institute of High Energy Physics, Chinese Academy of Science, Yuquan Road 19B, Shijingshan District, Beijing, People's Republic of China. *E-mail: lig@ihep.ac.cn

Synchrotron radiation computed laminography (SR-CL) has been in use in three-dimensional non-destructive imaging of flat objects for several years. A new set-up is proposed based on the traditional SR-CL method but with the detector inclined at the same angle as the sample inclination to collect projections. The results of computer simulations and real-sample experiments demonstrate that reconstructions acquired using an inclined detector are of better quality compared with those acquired using ordinary detecting methods, especially for the situation of few projections and small difference of attenuation ratio of the sample. This method could be applied to obtain high-quality images of weak-contrast samples with short measurement time and mild radiation damage.

Keywords: computed laminography; inclining detector.

1. Introduction

Since synchrotron radiation computed laminography (SR-CL) was first introduced to three-dimensional non-destructive imaging of flat objects by Helfen *et al.* (2005), it has been promoted by many researchers. The sampling volume in Fourier space for laminography was revealed and compared with traditional computed tomography (CT): the sampling volume is incomplete with two cone-shaped unsampled areas (Dobbins & Godfrey, 2003; Helfen *et al.*, 2005); compared with another incomplete sampling method, *i.e.* limited-angle CT, SR-CL has an advantage when the missing angular range is a significant fraction of the total angular range (Xu *et al.*, 2012). SR-CL was also applied to investigations of flip-chip bonded devices (Helfen *et al.*, 2007, 2011*a*), crack expansion of polymer composites (Moffat *et al.*, 2010; Xu *et al.*, 2010), ductile cracks in alloys (Morgeneyer *et al.*, 2011; Maire *et al.*, 2012; Shen *et al.*, 2013) and the microstructure of paint (Reischig *et al.*, 2013). It was also used in research of *Eupodophis descouensi* fossils to obtain images of hidden limbs (Houssaye *et al.*, 2011). Recently, SR-CL has been combined with microscopic and nano-imaging conditions (Hoshino *et al.*, 2011; Helfen *et al.*, 2013) and extended to neutron radiation (Helfen *et al.*, 20011*b*). Benefiting from the advancement of synchrotron radiation phase-contrast imaging (Snigirev *et al.*, 1995; Chapman *et al.*, 1997; David *et al.*, 2002), SR-CL has been associated with phase contrast in the non-destructive imaging of weak absorption-contrast material (Helfen *et al.*, 2009; Harasse *et al.*, 2010; Altapova *et al.*, 2012).

In traditional SR-CL, the normal of a two-dimensional X-ray detector is set parallel to the transmitting direction and kept at an inclined angle ($<90^\circ$) with the rotation axis. In this paper a new set-up is proposed: inclining the detector to make the normal of the detector parallel to the rotation axis of the sample. Computer simulations using digital models have been performed to investigate the differences in image reconstruction between the new set-up and ordinary SR-CL. Real-object experiments were also performed for comparison with the simulation results; we chose the algebraic reconstruction technique (ART) (Kak & Slaney, 1988) for image reconstruction and the condition of few projections.

2. Method

A sketch of the SR-CL set-up is shown in Fig. 1. In ordinary SR-CL, parallel X-rays are detected by a two-dimensional X-ray detector, which is set perpendicular to the X-ray transmitting direction, after penetrating through the sample with inclined angle θ. Although this inclination avoids the great difference in attenuation between the directions parallel and vertical to the sample surface, the projection along the Y-axis on the detector is compressed which degrades the resolution in the Y-direction. We propose a new SR-CL imaging set-up where the detector is inclined, making the normal of the detector parallel to the rotation axis. By this means, the area of the X-ray spot on the detector is extended along the Y-direction to make use of more pixels to acquire data, which recovers the compression of the projection along the Y-direction on the detector. This means more equations can be used in iterative calculations in the image reconstructions. The method promises to acquire better image quality with few projections. Based on the above analysis, computer simulations and real-object experiments were performed in order to make a comparison with the ordinary SR-CL method.

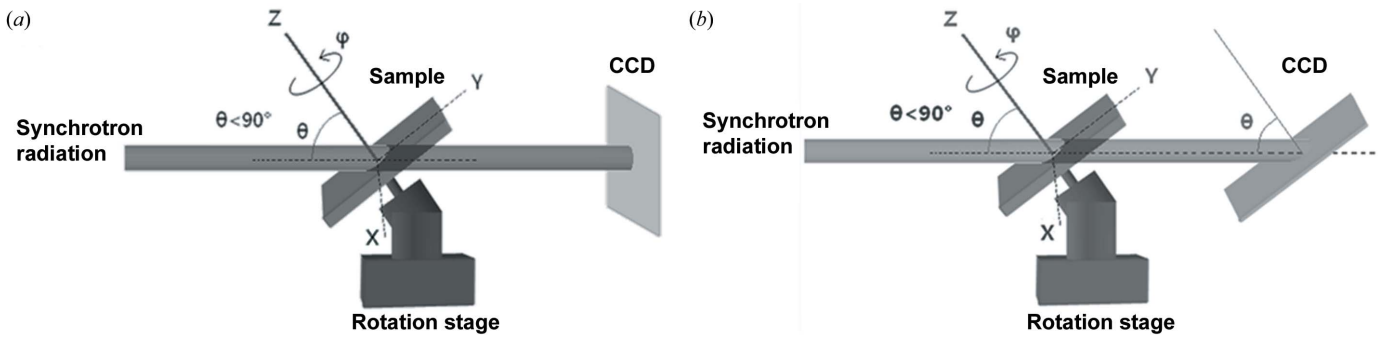

Figure 1
Geometry of the SR-CL with (*a*) the ordinary detecting method and (*b*) the inclining detector method.

3. Computer simulations

Details of the simulation model are shown in Fig. 2. It consists of 20 slices, with each slice containing 101 × 101 voxels with a certain value representing the mean absorption coefficient. The model is composed of three kinds of structures: 12 flat boards of different thickness and interspace inserted into the inner ten slices; another two flat boards containing 61 × 61 × 5 voxels embedded in the top and bottom five slices, and other parts of the model, the attenuation ratio of which is supposed to be 1.02:1.01:1 and 3:2:1 in the simulations. The 12 flat boards are divided into two groups located in perpendicular directions; each group contains three pairs of boards of respective thickness 5 voxels, 3 voxels and 1 voxel, and the interspaces are 5 voxels, 3 voxels and 1 voxel, respectively. The inclined angle is set to 45°. We choose projection data from a 71 × 51 pixel array for reconstruction under the condition of the ordinary detecting method and a 71 × 71 pixel array in the inclining method for the projection extension [51/cos(45) = 72.1] when the detector is inclined at 45°. The reconstructing volume is 121 × 121 × 20 voxels; time cost is about 56 s per iteration. We compared the reconstruction with two kinds of attenuation ratio and different projection numbers of 36 and 72. The reconstructive images obtained by ART are shown in Fig. 3.

The four groups of figures in Fig. 3 display the reconstruction of the tenth slice. Because the completely sampled area in the tenth slice is a circle area of diameter 51 voxels, in which the largest inscribed square is only 37 × 37 voxels in these settings, Fig. 3 only shows 37 × 37 voxels for each image. There are six pairs of images in each group with iterations of 1, 4, 10, 50, 100 and 400; each pair consists of one image obtained from the inclined detector and one acquired by the ordinary detecting method. From these figures it can be seen that the reconstructive images acquired by the inclining detector method have better quality than those obtained by the ordinary method for the same iterating cycles, especially for the situation of 36 projections and small difference of attenuation ratio of 1.02:1.01:1 between sample structures.

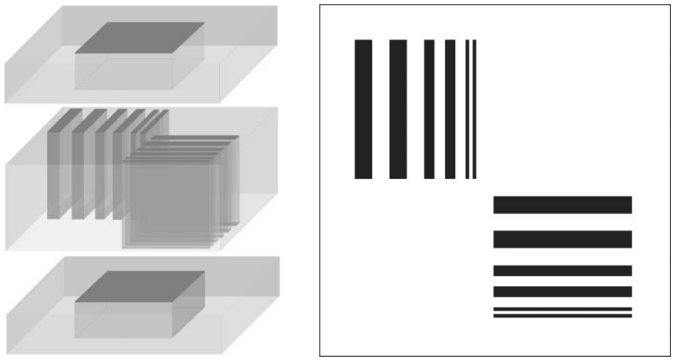

Figure 2
Sketch of the digital model and details of the middle slice.

In order to investigate the quality of the reconstruction images quantitatively, we took the smallest structure in the reconstruction image as the target (as shown in Fig. 4) to calculate the contrast to the background. This structure occupied an area of 18 × 1 pixels, and the adjacent area of 18 × 1 pixels was chosen as the background. We calculated the contrast of each pair of pixels, which consisted of one pixel from the smallest structure and one from its adjacent background, to obtain a mean value of the contrast. The results after 400 iterations are displayed in Table 1. It can be seen that the contrasts corresponding to the inclining detector method are better than those corresponding to the ordinary detecting method, whereas it is noticeable that, for the condition of 72 projections with a model attenuation ratio of 3:2:1, the discrepancy of contrast between these two types of detecting mode becomes very small.

The standard deviation (SD) of the contrast gradient of the smallest structure to the background was also investigated. We calculated the contrast of each pair of pixels and worked out the gradient of these contrast values, and then plotted the SD of the contrast gradient *versus* number of iterations. The results for the condition of 36 projections are displayed in Fig. 5 and the SDs of the contrast gradient after 400 iterations for all conditions are shown in Table 2. This shows that the SDs of the contrast gradients corresponding to the inclining detector method are smaller compared with those related to the ordinary detecting method after the same number of iterations. The results imply that the inclining detector method has an advantage in contrast uniformity over the ordinary detecting method.

We also calculated the gradient of the pixel values corresponding to the smallest structure, and then plotted the SD of

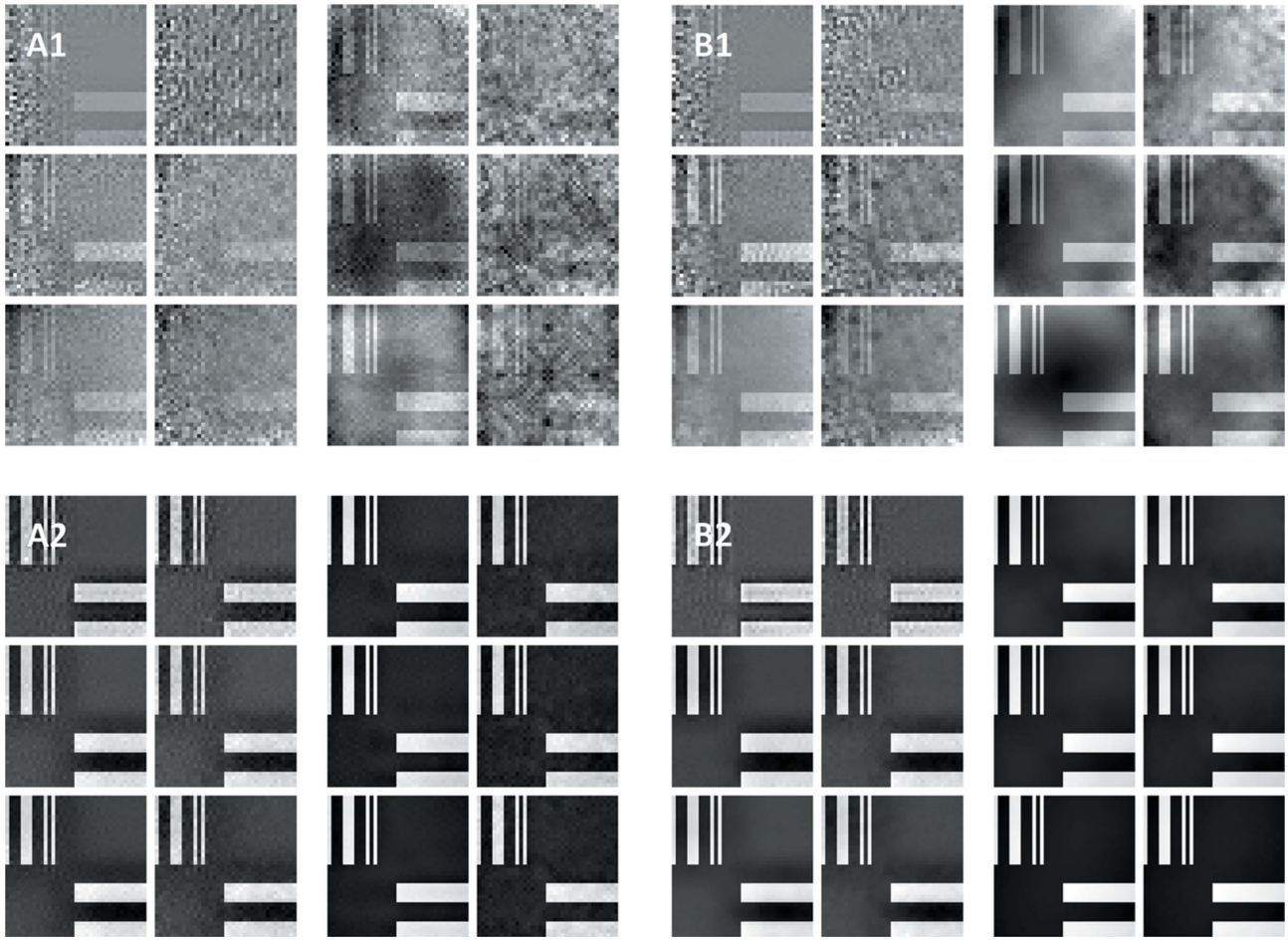

Figure 3
Reconstructive images of the tenth slice acquired using the inclining detector method and the ordinary method. Groups (A1) and (A2) are reconstructed with 36 projections related to attenuation ratios of 1.02:1.01:1 and 3:2:1, respectively, while (B1) and (B2) are reconstructed with 72 projections corresponding to the same attenuation ratio as (A1) and (A2). Each group contains six pairs of images, and the left-hand figure in each pair corresponds to the inclining detector method while the right-hand figure corresponds to the ordinary detecting method. Time cost is about 56 s per iteration.

the gradient *versus* number of iterations. The results for the condition of 36 projections are displayed in Fig. 6 and the SD of the pixel-value gradient after 400 iterations for all conditions are given in Table 3. This shows that the SD of the pixel-value gradient shows a similar behaviour to the SD of the contrast gradient in that the SDs corresponding to the inclining detector method show a lower value than those corresponding to the ordinary method, which means less variation in pixel value and greater smoothness.

4. Results and discussion

Real-object experiments of two kinds of sample based on two kinds of set-ups (see Fig. 1) were performed. The first object was a printed circuit board (PCB) of thickness $\sim$2 mm, inclined at an angle of 45°. The projections were acquired on beamline 13W1 of the Shanghai Synchrotron Radiation Facility with an X-ray energy of 25 keV obtained using a Si(111) double-crystal monochromator. The X-ray detector was a fibre-optic-coupled CCD camera from Photonic Science, on the front of which had been deposited a gadolinium oxysulphide X-ray scintillator of density $\sim$5 mg cm^{-2}; the pixel size of the CCD was 9 µm. The reconstruction was performed with ART using 36 projections, each projection containing 201 × 201 pixels, with reconstructing volume of 301 × 301 × 100 voxels and time cost of $\sim$13 min per iteration. The result is shown in Fig. 7. In order to investigate the difference in the smoothness of the pixel value and the contrast between the reconstructive images obtained *via* the two detecting methods directly, we traced the pixel values along a straight line located at the same position in the reconstructive images and then portrayed them as curves. The second object was a type of adhesive tape stuck to a thin transparent film of thickness $\sim$0.8 mm which was tested on beamline 4W1A of the Beijing Synchrotron Radiation Facility. The X-ray energy was 15 keV obtained from a Si(111) double-crystal monochromator. The X-ray detector was also a fibre-optic-coupled CCD camera from Photonic Science, the scintillator was made of GaOS:Tb of thickness $\sim$15 µm and the CCD pixel size was 7.4 µm. The attenuation ratio of structures in this sample was much smaller than for the PCB; we used 72 projections instead of 36 projections in image reconstruction,

Table 1
Contrast of the smallest structure in the image acquired using the inclining detector method and ordinary method under different conditions.

	36 projections		72 projections	
Detecting model	Attenuation ratio 1.02:1.01:1	Attenuation ratio 3:2:1	Attenuation ratio 1.02:1.01:1	Attenuation ratio 3:2:1
Inclined	0.0179	1.5451	0.0201	1.5435
Ordinary	0.0164	1.4840	0.0190	1.5431

Table 2
Standard deviation of the contrast gradient of the chosen area corresponding to the inclining detector method and ordinary method under different conditions after 400 iterations.

	36 projections		72 projections	
Detecting model	Attenuation ratio 1.02:1.01:1	Attenuation ratio 3:2:1	Attenuation ratio 1.02:1.01:1	Attenuation ratio 3:2:1
Inclined	0.0070	0.0435	0.0005	0.0038
Ordinary	0.0166	0.1474	0.0018	0.0068

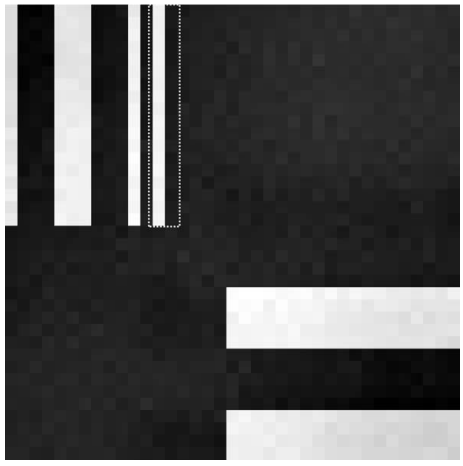

Figure 4
Sketch of the smallest structure (white) and its adjacent background (dark) for image quality evaluation. The related areas are highlighted by the dotted line.

each projection also containing 201 × 201 pixels, with reconstructing volume of 301 × 301 × 60 voxels and time cost of ∼12 min per iteration. The same method was used to investigate the image quality and the result is shown in Fig. 8.

Comparison of the reconstructive images obtained from the two types of detecting methods displayed in Figs. 7 and 8 indicates that images yielded from the inclined detector are smoother than those obtained by the ordinary method. The pixel-value curves show that curves corresponding to the inclined detector gave higher contrast in the boundary with less variation of pixel value compared with curves relating to the ordinary detecting method in the same iteration. It is demonstrated that the reconstructive images obtained using the inclining detector method have better quality for different attenuation ratio of structures which correspond well to the computer simulations.

According to the results of the simulations and experiments, reconstructions using the inclining detector method can improve the image quality with higher contrast and better smoothness compared with the ordinary detecting method, particularly for the situation of few projections and small difference of attenuation ratio of structures. This method could be applied to obtain high-quality images of weak-contrast samples with short measurement time and mild radiation damage.

Based on analysis by Guan & Gordon (1996), the number of projections can be evaluated from an unknown voxel number and the pixel number per projection used in the ART method. According to this method, projections used in simulations and real-sample experiments are underdetermined; however, since

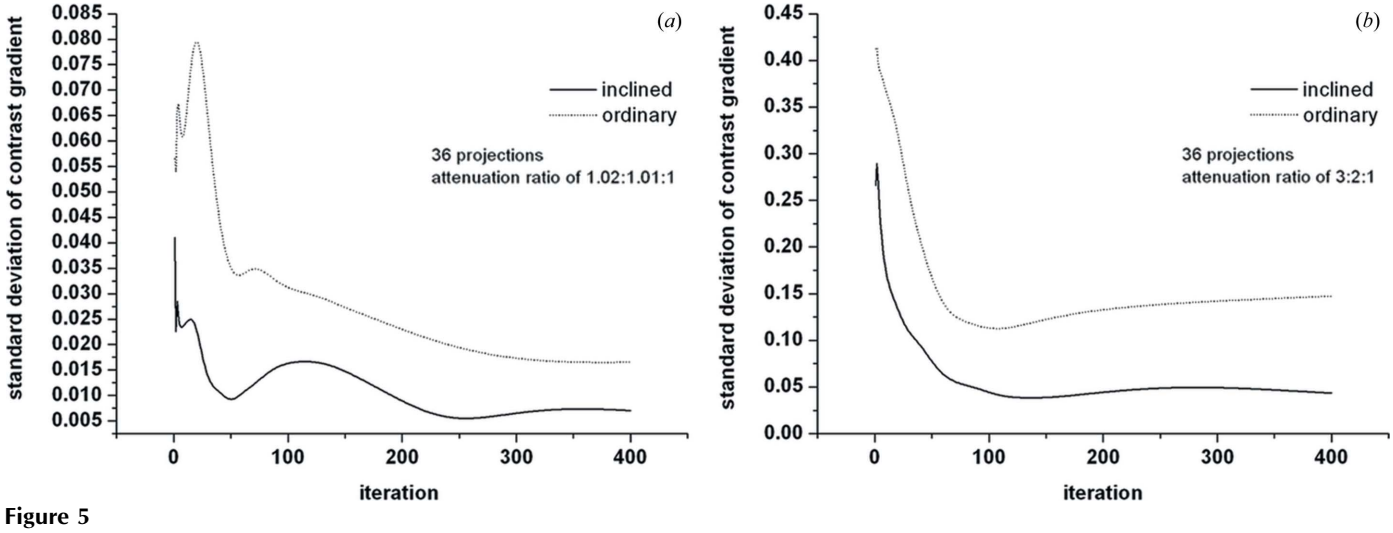

Figure 5
Standard deviation of the contrast gradient corresponding to the chosen area for the condition of 36 projections with attenuation ratio of (*a*) 1.02:1.01:1 and (*b*) 3:2:1.

our purpose here is to compare the inclining detector method and ordinary detecting method in terms of image quality, we omitted this in this article by focusing on the discrepancy of the reconstruction quality under different conditions.

It should be noted that the advantage of the inclining detector method will be reduced for higher contrast and more projections. This is probably because the increasing correction by using more pixels to collect projections due to the inclining detector becomes less significant with increasing projection number, and the sensitivity to the pixel-value correction will also be degraded with increasing sample contrast. Although the inclining detector method increases the sampling frequency along the *Y*-direction (as depicted in Fig. 1) compared with the ordinary detecting method, which

Table 3
Standard deviation of the pixel-value gradient of the smallest structure corresponding to the inclining detector method and the ordinary method under different conditions after 400 iterations.

	36 projections		72 projections	
Detecting model	Attenuation ratio 1.02:1.01:1	Attenuation ratio 3:2:1	Attenuation ratio 1.02:1.01:1	Attenuation ratio 3:2:1
Inclined	0.0051	0.0153	0.0004	0.0020
ordinary	0.0129	0.0752	0.0014	0.0041

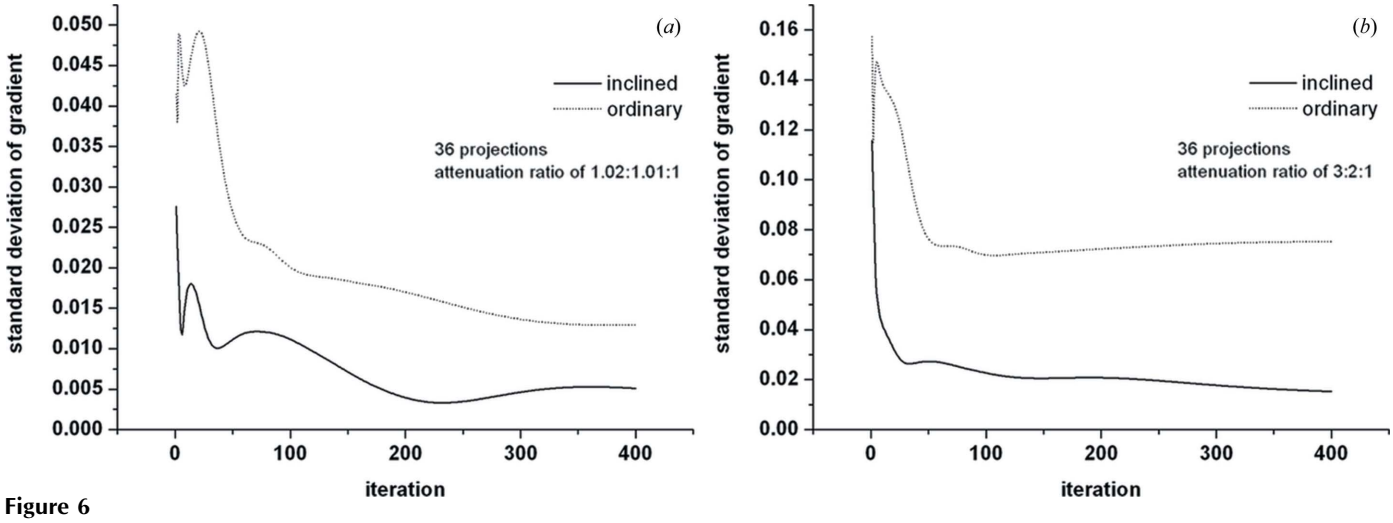

Figure 6
Standard deviation of the pixel-value gradient of the smallest structure corresponding to the inclining detector method and the ordinary method for the condition of 36 projections with attenuation ratio of (*a*) 1.02:1.01:1 and (*b*) 3:2:1.

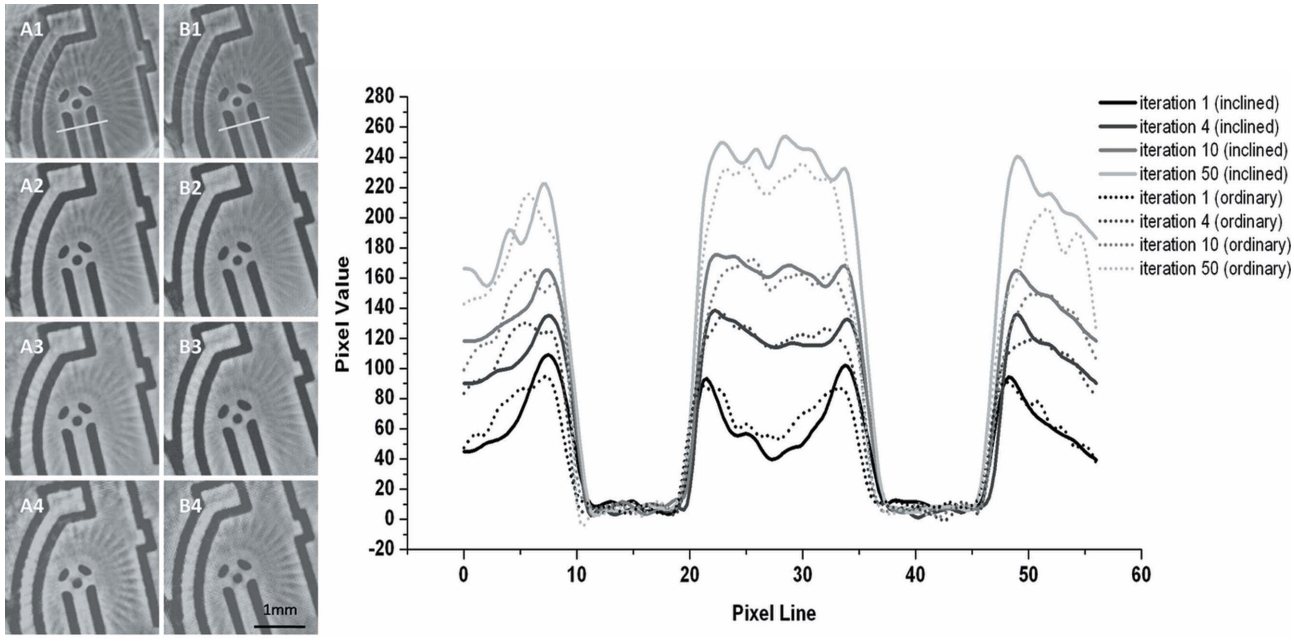

Figure 7
Reconstructive images of PCB and the curves of pixel value along the white line. (A1)–(A4) were acquired using the inclined detector method, (B1)–(B4) were acquired using the ordinary detecting method; some radial artifacts can be seen in the images due to few projections used in the reconstruction. The number of iterations for each pair are 1, 4, 10 and 50, respectively. Time cost is ~13 min per iteration.

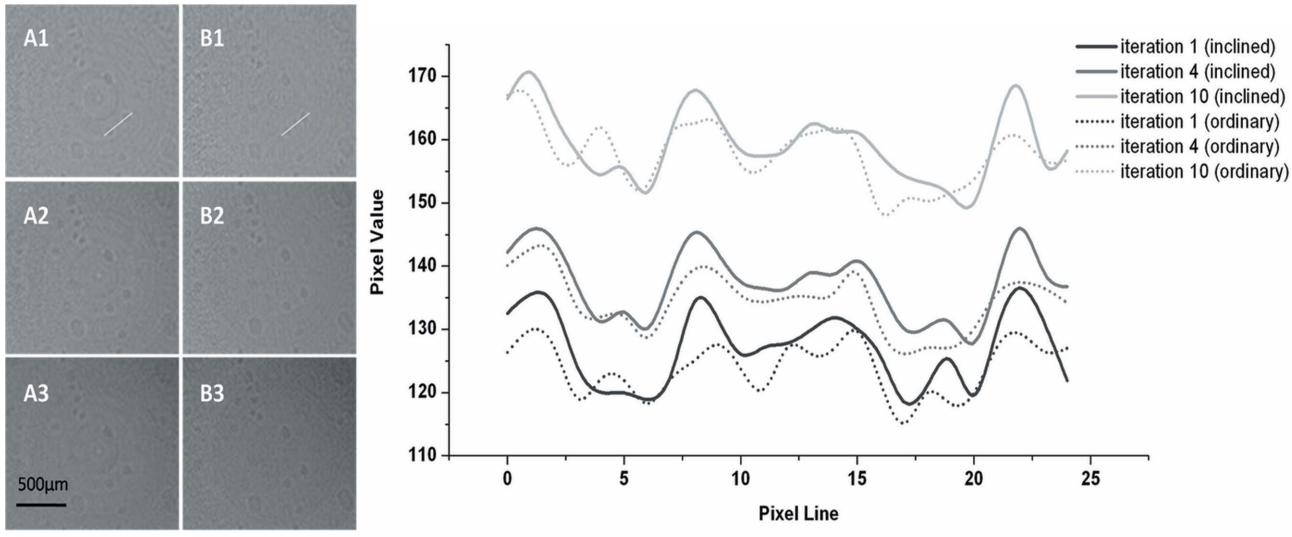

Figure 8
Reconstructive images of adhesive tape and the curves of pixel value along the white line which crosses two air bubbles. (A1)–(A3) were acquired using the inclined detector method, (B1)–(B3) were acquired using the ordinary detecting method. The number of iterations of each pair are 1, 4 and 10, respectively. Time cost is ∼12 min per iteration.

benefits image reconstruction, it makes no change in the interaction of X-rays and specimen; the cone-shaped unsampled areas in reciprocal space coherent to laminography still exist, which will affect the image quality in the filtered back-projection method. The increasing sampling frequency is expected to make appropriate improvement of the spatial resolution along the rotation axis of the sample in the ART method; however, artifacts due to image overlaps of different slices have a negative effect on the spatial resolution along the rotation axis, which requires further investigation.

Additionally, the X-ray detector with scintillator is always fibre-optic-coupled or lens-coupled; there will be little effect to detective efficiency and resolution in the inclining detector method with fibre-optic-coupled and thin-scintillator detector in high-resolution imaging, while it may have a significant effect with a thick-scintillator lens-coupled detector of blurring the projections with resolution degraded.

This work was supported by National Science Foundation of China grants 60972116 and 41023008. We thank Beijing Synchrotron Radiation Facility (4W1A) and Shanghai Synchrotron Radiation Facility (BL13W1) for beam time access.

References

Altapova, V., Helfen, L., Myagotin, A., Hänschke, D., Moosmann, J., Gunneweg, J. & Baumbach, T. (2012). *Opt. Express*, **20**, 6496–6508.
Chapman, D., Thomlinson, W., Johnston, R. E., Washburn, D., Pisano, E., Gmür, N., Zhong, Z., Menk, R., Arfelli, F. & Sayers, D. (1997). *Phys. Med. Biol.* **42**, 2015–2025.
David, C., Nöhammer, B., Solak, H. H. & Ziegler, E. (2002). *Appl. Phys. Lett.* **81**, 3287–3289.
Dobbins, J. T. & Godfrey, D. J. (2003). *Phys. Med. Biol.* **48**, R65–R106.
Guan, H. & Gordon, R. (1996). *Phys. Med. Biol.* **41**, 1727–1743.
Harasse, S., Hirayama, N., Yashiro, W. & Momose, A. (2010). *Proc. SPIE*, **7804**, 780411.
Helfen, L., Baumbach, T., Cloetens, P. & Baruchel, J. (2009). *Appl. Phys. Lett.* **94**, 104103.
Helfen, L., Baumbach, T., Mikulík, P., Kiel, D., Pernot, P., Cloetens, P. & Baruchel, J. (2005). *Appl. Phys. Lett.* **86**, 071915.
Helfen, L., Myagotin, A., Mikulík, P., Pernot, P., Voropaev, A., Elyyan, M., Di Michiel, M., Baruchel, J. & Baumbach, T. (2011*a*). *Rev. Sci. Instrum.* **82**, 063702.
Helfen, L., Myagotin, A., Rack, A., Pernot, P., Mikulík, P., Di Michiel, M. & Baumbach, T. (2007). *Phys. Status Solidi A*, **204**, 2760–2765.
Helfen, L., Xu, F., Schillinger, B., Calzada, E., Zanette, I., Weitkamp, T. & Baumbach, T. (2011*b*). *Nucl. Instrum. Methods Phys. Res. A*, **651**, 135–139.
Helfen, L., Xu, F., Suhonen, H., Urbanelli, L., Cloetens, P. & Baumbach, T. (2013). *J. Instrum.* **8**, C05006.
Hoshino, M., Uesugi, K., Takeuchi, A., Suzuki, Y. & Yagi, N. (2011). *Rev. Sci. Instrum.* **82**, 073706.
Houssaye, A., Xu, F., Helfen, L., De Buffrénil, V., Baumbach, T. & Tafforeau, P. (2011). *J. Vertebrate Paleontol.* **31**, 2–7.
Kak, A. C. & Slaney, M. (1988). *Principles of Computerized Tomographic Imaging.* Piscataway: IEEE Press.
Maire, E., Morgeneyer, T., Landron, C., Adrien, J. & Helfen, L. (2012). *C. R. Phys.* **13**, 328–336.
Moffat, A. J., Wright, P., Helfen, L., Baumbach, T., Johnson, G., Spearing, S. M. & Sinclair, I. (2010). *Scr. Mater.* **62**, 97–100.
Morgeneyer, T. F., Helfen, L., Sinclair, I., Proudhon, H., Xu, F. & Baumbach, T. (2011). *Scr. Mater.* **65**, 1010–1013.
Reischig, P., Helfen, L., Wallert, A., Baumbach, T. & Dik, J. (2013). *Appl. Phys. A*, **111**, 983–995.
Shen, Y., Morgeneyer, J., Garnier, L., Allais, L., Helfen, L. & Crépin, J. (2013). *Acta Mater.* **61**, 2571–2582.
Snigirev, A., Snigireva, I., Kohn, V., Kuznetsov, S. & Schelokov, I. (1995). *Rev. Sci. Instrum.* **66**, 5486–5492.
Xu, F., Helfen, L., Baumbach, T. & Suhonen, H. (2012). *Opt. Express*, **20**–2, 794–806.
Xu, F., Helfen, L., Moffat, A. J., Johnson, G., Sinclair, I. & Baumbach, T. (2010). *J. Synchrotron Rad.* **17**, 222–226.